

Spin-Dependent Electron Transport through Bacterial Cell Surface Multiheme Electron Conduits

Suryakant Mishra,^{‡#} Sahand Pirbadian,^{‡#} Amit Kumar Mondal,[†] Mohamed Y. El-Naggar,^{*‡||§} and Ron Naaman^{*†}

[†] Department of Chemical and Biological Physics, Weizmann Institute of Science, Rehovot 76100, Israel

[‡] Department of Physics and Astronomy, University of Southern California, Los Angeles, California 90089, United States

^{||} Department of Chemistry, University of Southern California, Los Angeles, California 90089, United States

[§] Department of Biological Sciences, University of Southern California, Los Angeles, California 91030, United States

ABSTRACT: Multiheme cytochromes, located on the bacterial cell surface, function as long-distance (> 10 nm) electron conduits linking intracellular reactions to external surfaces. This extracellular electron transfer process, which allows microorganisms to gain energy by respiring solid redox-active minerals, also facilitates the wiring of cells to electrodes. While recent studies suggested that a chiral induced spin selectivity effect is linked to efficient electron transmission through biomolecules, this phenomenon has not been investigated in the extracellular electron conduits. Using magnetic conductive probe atomic force microscopy, Hall voltage measurements, and spin-dependent electrochemistry of the decaheme cytochromes MtrF and OmcA from the metal-reducing bacterium *Shewanella oneidensis* MR-1, we show that electron transport through these extracellular conduits is spin-selective. Our study has implications for understanding how spin-dependent interactions and magnetic fields may control electron transport across biotic-abiotic interfaces in both natural and biotechnological systems.

Electron flow dictates all biological energy conversion strategies.^{1,2} In the case of respiration, cells harvest energy by controlling electron flow from electron donors (fuels) to terminal electron acceptors (oxidants) through a

chain of reduction-oxidation (redox) cofactors. Some microorganisms (including metal-reducing bacteria) can also extend this electron transport chain to terminal acceptors *outside* the cells, allowing anaerobic respiration of solid minerals in the absence of soluble oxidants (e.g. O₂) that enter the cells.³ This extracellular electron transfer (EET) strategy also facilitates the ‘wiring’ of cells to solid-state electrodes in a number of renewable energy (microbial fuel cells and electrosynthesis) and bioelectronic technologies.⁴⁻⁷

The metal-reducing bacterium *Shewanella oneidensis* MR-1 expresses a network of multiheme cytochromes (MHCs), known as the Mtr-Omc pathway, to accomplish EET across the biotic-abiotic interface.⁸ As part of this pathway, decaheme cytochromes located on the cell surface (MtrC, MtrF, OmcA), can transmit electrons from periplasmic redox partners to the extracellular space.⁹⁻¹¹ Measurements¹²⁻¹⁴ and quantum/molecular simulations^{8,15} revealed rapid electron hopping rates through the *S. oneidensis* multiheme conduits, sufficiently high to meet the cellular EET rate.¹⁶ These cytochromes can also facilitate long-distance (micrometer scale) redox conduction along cellular membranes.¹⁷ Rapid electron flux (10⁵ s⁻¹) through the solvated decaheme cytochromes is thought to arise from the packing of hemes into wire-like chains, presence of cysteine linkages that enhance electronic couplings, and careful control of the redox potential landscape.^{8,15,18,19} Solid-state (vacuum) measurements in monolayer junctions of the MHCs also revealed remarkable temperature-independent electronic conduction (0.3 A cm⁻² at 50 mV for MtrF), on par with conjugated organics, suggesting a heme-assisted coherent tunneling mechanism.²⁰

An additional factor that may enhance the electron transport efficiency in biological systems has recently been observed: chiral induced spin selectivity (CISS), an effect that couples the electron’s spin to its linear momentum in a chiral potential, including nucleic acids and proteins.^{21,22} This property enhances the transmission probability of one preferred spin, dependent on the chirality of the molecule, and suppresses backscattering.

Given the observations of efficient electron flux in bacterial MHCs, we hypothesized that electron transport through these proteins could accompany spin selectivity. CISS in MHCs could potentially give rise to spin effects in the biotic-abiotic interaction between cells and solid phase electron donors/acceptors, especially those with magnetic properties, or in electron-exchange processes involving other chiral biomolecules, such as electron shuttling or interspecies electron transfer. In addition, CISS in MHCs may provide a basis for understanding the reported magnetic field effect on the performance of microbial fuel cells,²³⁻²⁶ including those catalyzed by *S. oneidensis*. The latter observations have so far been tentatively assigned to oxidative stress or

magnetohydrodynamic effects, but the role of the electron spin has not been investigated.

Here, we investigated and confirmed the role of spin in electron transport through the *S. oneidensis* MR-1 outer membrane decaheme cytochromes MtrF and OmcA. To monitor electron transport, extent of spin polarization in the transferred electrons, and spin-dependent polarizability in the proteins, we applied various experimental techniques previously used to demonstrate CISS in DNA, oligopeptides, and chiral polymers: solvent-free magnetic conductive probe atomic force microscopy (mCP-AFM), Hall voltage measurements along with spin-dependent electrochemistry of the proteins in solution.²⁷⁻³¹

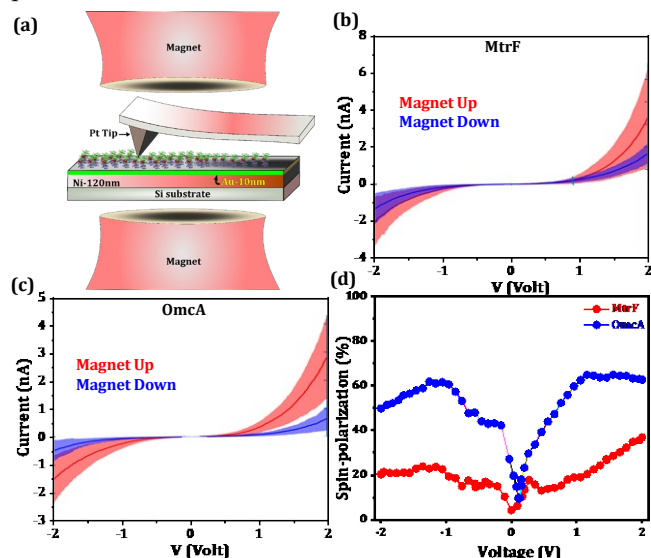


Figure 1. Spin-dependent conduction study of MtrF and OmcA by mCP-AFM. (a) Scheme of the measurement, (b & c) I - V plots of MtrF and OmcA, respectively where Ni film magnetized with the north pole pointing up (red) or down (blue). (d) The corresponding percentage of spin-polarization (SP) $\{(I_{up} - I_{down}) / (I_{up} + I_{down})\} \times 100$ for MtrF and OmcA, respectively. Here I_{up} and I_{down} are the currents with magnetic north pole up and down, respectively. (Note: panels b) and c), width of the lines represents the standard deviation of the measurements.)

Using mCP-AFM, we measured electron transmission through solvent-free MtrF and OmcA adsorbed on a ferromagnetic Ni, 120nm thick substrate coated with a thin (10 nm) Au layer. MtrF and OmcA were effectively immobilized on the surface through covalent thiol bonds with Au as a result of a recombinant tetra-cysteine tag at the C-terminus of the proteins, as described in previous scanning probe studies¹⁴ and confirmed here (Figure S2). Nonmagnetic (Pt) tips functioned as the top electrodes and conduction was measured with magnetic fields pointing either with the north pole up or down (UP or DOWN) using a permanent magnet that determines the spin alignment in the Ni bottom substrate.^{28,32} Current-voltage (I - V) spectra were acquired from multiple points

on each of the monolayers, revealing a magnitude and voltage dependence consistent with previous tunneling spectroscopy measurements of both proteins.^{12,14}

Figure 1 shows clear spin selectivity in both proteins, with higher conductivity when the magnetic field is pointing ‘UP’ compared to ‘DOWN’. The extent of SP at a given voltage can be quantified using the ratio $(I_{UP} - I_{DOWN}) / (I_{UP} + I_{DOWN})$, where I_{UP} and I_{DOWN} are the currents associated with the two different magnetic field directions. As can be seen in Figure 1d, OmcA displayed the higher SP ($63 \pm 2\%$) compared to MtrF ($37 \pm 3\%$) at 2.0 V bias.

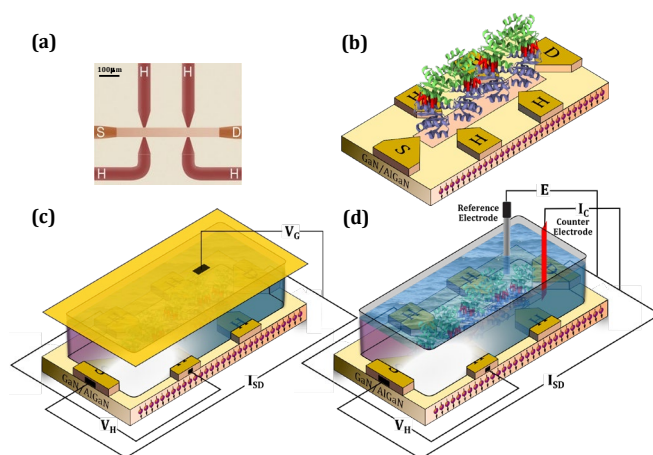


Figure 2. (a) Optical microscopic image of the Hall device patterned on GaN/AlGaIn substrate. (b) A scheme of the Hall device on which a monolayer of the protein is adsorbed. (c) A scheme of the setup used for measuring spin polarization. A Hall device coated with monolayer of proteins is covered by buffer electrolyte with top gate electrode insulated from the solution. (d) Spin-dependent electrochemistry setup where Hall device used as the working electrode measures the faradaic current flows through the protein monolayer and Hall potential.

In addition to the solid-state (solvent-free) mCP-AFM measurements, we also measured the Hall voltage resulting from the spin polarizability that accompanies charge polarization across MtrF and OmcA in solution (see SI for details). The measurement system (Figure 2) is based on Au-coated (5 nm film) Hall device patterned on a GaN/AlGaIn two-dimensional electron gas structure.^{29,30} In addition to allowing thiol-binding, the Au film stabilizes the potential on the surface by eliminating surface states.³⁰ With a constant current driven between the source and drain electrodes, a voltage is applied between a top gate electrode and the device on which the proteins are placed. The gate voltage generates an electric field that induces charge polarization perpendicular to the protein monolayer. If this charge polarization is accompanied by spin polarization, a magnetic field is created and a Hall voltage is measured across the lateral Hall probes (Figure 2). Prior to Hall voltage measurements, the attachment of the MtrF and OmcA protein monolayers were confirmed with liquid

tapping mode atomic force microscopy and polarization modulation-infrared reflection-absorption spectroscopy (Figure S2 and S3).

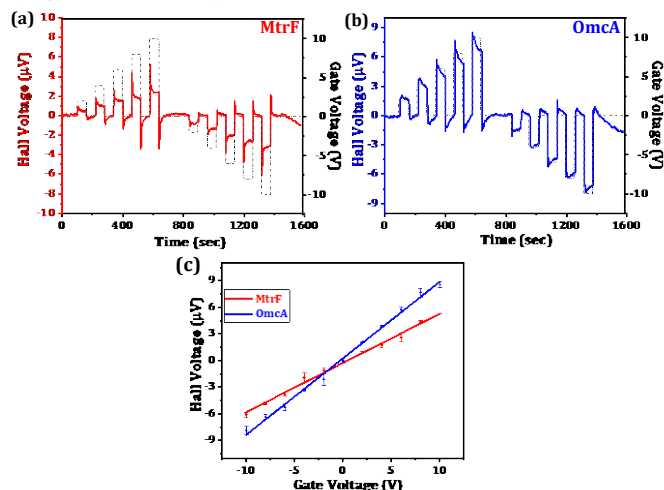


Figure 3. The spin polarizability measured as a function of the potential applied (dotted black line) on the top gate of gold (Fig. 2C) for (a) device coated with MtrF and (b) device coated with OmcA. (c) The Hall signal as a function of the gate voltage applied for devices coated with MtrF (red) and OmcA (blue). A linear response is observed and OmcA having higher spin polarizability compared to MtrF.

Figure 3(a, b) shows the Hall voltages observed in response to gate voltage steps of different magnitudes and signs for both MtrF and OmcA. This data confirm that the spin polarization indeed accompanies the field-induced charge polarization in both MHCs. The Hall signals scale linearly with the gate voltage (Figure 3c) and, consistent with the mCP-AFM measurements, the spin polarization is larger for OmcA as compared to MtrF. By comparing to a separate calibration of the Hall devices using external magnetic fields (see Figure S4 in SI), the OmcA Hall signal at 10 V gate voltage corresponds to a magnetic field of about 200 Gauss. To verify the importance of the secondary/tertiary structure in the observed spin polarization effect, the proteins were denatured at 80 °C (see SI for details), after which no spin polarization was observed in response to gate voltage (Figure S5).

It is interesting to consider the possible reasons leading to higher spin polarization in OmcA relative to MtrF. The two MHCs have comparable conductivities (with MtrF transmitting slightly higher current in mCP-AFM measurements, Figure 1), so it is unlikely that the observed higher spin polarization of OmcA is the result of overall higher electron transmission. Another factor that may contribute to the magnitude of spin polarization in the Hall device measurements is the protein size, since the electric dipole moment induced by the electric field depends on the size of the protein. At 83 kDa, OmcA is moderately bulkier than MtrF (74 kDa).⁸ However, a comparison of the X-ray structures shows similar overall dimensions, particularly along the directions of the charge carrier octa-heme and tetra-heme chains that define the

staggered cross configuration common to both proteins.^{33,34} Therefore, we conclude that differences in overall size are a less likely explanation for the significant difference in spin selectivity. A more detailed comparison of the secondary structures, however, may offer clues. For example, α -helices serve as primary scaffolds for hemes in both proteins, but OmcA has a significantly higher helical secondary structure (18%) than MtrF (11%) when compared using the DSSP tool.³⁵ Figure S6 highlights the increased helical content in the heme-containing domains II and IV of OmcA compared to MtrF. We therefore hypothesize that the difference in the secondary structure surrounding the electron carrying heme chains plays an important role in determining the extent of the spin selectivity.

In a third experimental approach, we performed spin-dependent electrochemical measurements as previously applied to DNA and oligopeptide.^{30,31} Here, the measurements are performed in standard 3-electrode electrochemical cells with the Hall device serving as the working electrode. While performing cyclic voltammetry (CV), the Hall potential is monitored simultaneously, so as to obtain information on the spin selectivity of the process (Figure S7a&b). In addition to the reductive and oxidative electrochemical signatures observed in the CVs of MtrF and OmcA, a simultaneous Hall potential signal reflecting spin selectivity associated with the electron transfer through both proteins (Figure S7b). It is interesting to note that the electrochemical potentials of MtrF and OmcA are shifted relative to previous reports,^{33,36,37} which we attribute to the cysteine-based immobilization strategy and the use of bare thin gold electrodes, rather than adsorption on graphite or self-assembled monolayers, since the immobilization procedure is known to influence the measured redox properties.³⁷ Consistent with both the mCP-AFM (Figure 1) and field-induced polarization measurements (Figure 3), higher spin selectivity was observed for OmcA, compared to MtrF, in the electrochemical measurements (Figure S7a&b). Denaturation of the proteins resulted in significant decrease of electrochemical current and corresponding order of magnitude reduction in the Hall signal (Figure S7c-f), again confirming the role of the protein's structure in dictating the spin selectivity process associated with electron transmission.

The spin selectivity observed in the extracellular bacterial cytochromes may have interesting implications for controlling electron transfer across the biotic-abiotic interface. It was recently proposed that such spin selectivity may place constraints on the ability to interact with other chiral molecules.²⁹ In the case of EET conduits, this effect may lead to selectivity in interactions with electron exchange partners, such as soluble redox shuttles or neighboring electron conduits of other cells. We also speculate that spin selectivity may play a role in controlling interactions with external electron accepting minerals, such as certain iron oxides, that have magnetic

properties. Finally, spin polarization offers a concrete mechanism that may impact our understanding of multiple recent reports²³⁻²⁶ describing magnetic field enhancements of EET in microbial fuel cells.

To summarize, we have found that electron flow in the *Shewanella oneidensis* MR-1 cell surface decaheme cytochromes is spin selective. This observation opens up an additional degree of freedom, based on electron spin, for controlling charge transport across biotic-abiotic interfaces in both natural (environmental) systems and biotechnological (e.g. renewable energy or bioelectronic) applications.

AUTHOR INFORMATION

Corresponding Authors

* mnagggar@usc.edu, ron.naaman@weizmann.ac.il

Author Contributions

These authors contributed equally.

Notes

The authors declare no competing financial interests.

ACKNOWLEDGMENT

M.Y.E.-N. and S.P. acknowledge support by the U.S. Office of Naval Research Multidisciplinary University Research Initiative Grant No. N00014-18-1-2632. We are grateful to Prof. Liang Shi (China University of Geoscience in Wuhan) for supplying the MtrF and OmcA constructs. RN acknowledges the support of the Templeton Foundation and of the Israel Science Foundation.

References

- (1) Gray, H. B.; Winkler, J. R. Electron Tunneling through Proteins. *Q Rev Biophys* **2003**, *36* (3), 341–372. <https://doi.org/10.1017/S0033583503003913>.
- (2) Beratan, D. N.; Liu, C. R.; Migliore, A.; Polizzi, N. F.; Skourtis, S. S.; Zhang, P.; Zhang, Y. Q. Charge Transfer in Dynamical Biosystems, or The Treachery of (Static) Images. *Accounts Chem Res* **2015**, *48* (2), 474–481. <https://doi.org/10.1021/ar500271d>.
- (3) Shi, L.; Dong, H. L.; Reguera, G.; Beyenal, H.; Lu, A. H.; Liu, J.; Yu, H. Q.; Fredrickson, J. K. Extracellular Electron Transfer Mechanisms between Microorganisms and Minerals. *Nat Rev Microbiol* **2016**, *14* (10), 651–662. <https://doi.org/10.1038/nrmicro.2016.93>.
- (4) Lienemann, M.; TerAvest, M. A.; Pitkanen, J. P.; Stuns, I.; Penttila, M.; Ajo-Franklin, C. M.; Jantti, J. Towards Patterned Bioelectronics: Facilitated Immobilization of Exoelectrogenic Escherichia Coli with Heterologous Pili. *Microb Biotechnol* **2018**, *11* (6), 1184–1194. <https://doi.org/10.1111/1751-7915.13309>.
- (5) Sakimoto, K. K.; Kornienko, N.; Cestellos-Blanco, S.; Lim, J.; Liu, C.; Yang, P. D. Physical Biology of the Materials-Microorganism Interface. *J Am Chem Soc* **2018**, *140* (6), 1978–1985. <https://doi.org/10.1021/jacs.7b11135>.
- (6) Logan, B. E.; Rossi, R.; Ragab, A.; Saikaly, P. E. Electroactive Microorganisms in Bioelectrochemical Systems. *Nat Rev Microbiol* **2019**, *17* (5), 307–319. <https://doi.org/10.1038/s41579-019-0173-x>.
- (7) Su, L.; Ajo-Franklin, C. M. Reaching Full Potential: Bioelectrochemical Systems for Storing Renewable Energy in Chemical Bonds. *Current Opinion in Biotechnology* **2019**, *57*, 66–72. <https://doi.org/10.1016/j.copbio.2019.01.018>.
- (8) Breuer, M.; Rosso, K. M.; Blumberger, J.; Butt, J. N. Multi-Haem Cytochromes in Shewanella Oneidensis MR-1: Structures, Functions and Opportunities. *J R Soc Interface* **2015**, *12* (102). <https://doi.org/ARTN2014111710.1098/rsif.2014.1117>.
- (9) Hartshorne, R. S.; Reardon, C. L.; Ross, D.; Nuester, J.; Clarke, T. A.; Gates, A. J.; Mills, P. C.; Fredrickson, J. K.; Zachara, J. M.; Shi, L.; et al. Characterization of an Electron Conduit between Bacteria and the Extracellular Environment. *P Natl Acad Sci USA* **2009**, *106* (52), 22169–22174. <https://doi.org/10.1073/pnas.0900086106>.
- (10) Bucking, C.; Popp, F.; Kerzenmacher, S.; Gescher, J. Involvement and Specificity of Shewanella Oneidensis Outer Membrane Cytochromes in the Reduction of Soluble and Solid-Phase Terminal Electron Acceptors. *Fems Microbiol Lett* **2010**, *306* (2), 144–151. <https://doi.org/10.1111/j.1574-6968.2010.01949.x>.
- (11) Coursolle, D.; Baron, D. B.; Bond, D. R.; Gralnick, J. A. The Mtr Respiratory Pathway Is Essential for Reducing Flavins and Electrodes in Shewanella Oneidensis. *J Bacteriol* **2010**, *192* (2), 467–474. <https://doi.org/10.1128/Jb.00925-09>.
- (12) Wigginton, N. S.; Rosso, K. M.; Hochella, M. F. Mechanisms of Electron Transfer in Two Decaheme Cytochromes from a Metal-Reducing Bacterium. *J Phys Chem B* **2007**, *111* (44), 12857–12864. <https://doi.org/10.1021/jp0718698>.
- (13) White, G. F.; Shi, Z.; Shi, L.; Wang, Z. M.; Dohnalkova, A. C.; Marshall, M. J.; Fredrickson, J. K.; Zachara, J. M.; Butt, J. N.; Richardson, D. J.; et al. Rapid Electron Exchange between Surface-Exposed Bacterial Cytochromes and Fe(III) Minerals. *P Natl Acad Sci USA* **2013**, *110* (16), 6346–6351. <https://doi.org/10.1073/pnas.1220074110>.
- (14) Byun, H. S.; Pirbadian, S.; Nakano, A.; Shi, L.; El-Naggar, M. Y. Kinetic Monte Carlo Simulations and Molecular Conductance Measurements of the Bacterial Decaheme Cytochrome MtrF. *Chemelectrochem* **2014**, *1* (11), 1932–1939. <https://doi.org/10.1002/celec.201402211>.

- (15) Jiang, X. Y.; Burger, B.; Gajdos, F.; Bortolotti, C.; Futera, Z.; Breuer, M.; Blumberger, J. Kinetics of Trifurcated Electron Flow in the Decaheme Bacterial Proteins MtrC and MtrF. *P Natl Acad Sci USA* **2019**, *116* (9), 3425–3430. <https://doi.org/10.1073/pnas.1818003116>.
- (16) Gross, B. J.; El-Naggar, M. Y. A Combined Electrochemical and Optical Trapping Platform for Measuring Single Cell Respiration Rates at Electrode Interfaces. *Rev Sci Instrum* **2015**, *86* (6). [https://doi.org/Artn 064301 10.1063/1.4922853](https://doi.org/Artn%20064301%2010.1063/1.4922853).
- (17) Xu, S.; Barrozo, A.; Tender, L. M.; Krylov, A. I.; El-Naggar, M. Y. Multiheme Cytochrome Mediated Redox Conduction through *Shewanella Oneidensis* MR-1 Cells. *J Am Chem Soc* **2018**, *140* (32), 10085–10089. <https://doi.org/10.1021/jacs.8b05104>.
- (18) Breuer, M.; Rosso, K. M.; Blumberger, J. Electron Flow in Multiheme Bacterial Cytochromes Is a Balancing Act between Heme Electronic Interaction and Redox Potentials. *P Natl Acad Sci USA* **2014**, *111* (2), 611–616. <https://doi.org/10.1073/pnas.1316156111>.
- (19) Barrozo, A.; El-Naggar Mohamed, Y.; Krylov Anna, I. Distinct Electron Conductance Regimes in Bacterial Decaheme Cytochromes. *Angewandte Chemie International Edition* **2018**, *57* (23), 6805–6809. <https://doi.org/10.1002/anie.201800294>.
- (20) Garg, K.; Ghosh, M.; Eliash, T.; van Wonderen, J. H.; Butt, J. N.; Shi, L.; Jiang, X. Y.; Zdenek, F.; Blumberger, J.; Pecht, I.; et al. Direct Evidence for Heme-Assisted Solid-State Electronic Conduction in Multi-Heme c-Type Cytochromes. *Chem Sci* **2018**, *9* (37). <https://doi.org/10.1039/c8sc01716f>.
- (21) Michaeli, K.; Kantor-Uriel, N.; Naaman, R.; Waldeck, D. H. The Electron's Spin and Molecular Chirality - How Are They Related and How Do They Affect Life Processes? *Chem Soc Rev* **2016**, *45* (23), 6478–6487. <https://doi.org/10.1039/c6cs00369a>.
- (22) Naaman, R.; Paltiel, Y.; Waldeck, D. H. Chiral Molecules and the Electron Spin. *Nature Reviews Chemistry* **2019**, *3* (4), 250–260. <https://doi.org/10.1038/s41570-019-0087-1>.
- (23) Li, W. W.; Sheng, G. P.; Liu, X. W.; Cai, P. J.; Sun, M.; Xiao, X.; Wang, Y. K.; Tong, Z. H.; Dong, F.; Yu, H. Q. Impact of a Static Magnetic Field on the Electricity Production of *Shewanella*-Inoculated Microbial Fuel Cells. *Biosens Bioelectron* **2011**, *26* (10), 3987–3992. <https://doi.org/10.1016/j.bios.2010.11.027>.
- (24) Yin, Y.; Huang, G. T.; Tong, Y. R.; Liu, Y. D.; Zhang, L. H. Electricity Production and Electrochemical Impedance Modeling of Microbial Fuel Cells under Static Magnetic Field. *J Power Sources* **2013**, *237*, 58–63. <https://doi.org/10.1016/j.jpowsour.2013.02.080>.
- (25) Li, C.; Wang, L. G.; Liu, H. Enhanced Redox Conductivity and Enriched Geobacteraceae of Exoelectrogenic Biofilms in Response to Static Magnetic Field. *Appl Microbiol Biot* **2018**, *102* (17), 7611–7621. <https://doi.org/10.1007/s00253-018-9158-3>.
- (26) Zhou, H. H.; Mei, X. X.; Liu, B. F.; Xie, G. J.; Xing, D. F. Magnet Anode Enhances Extracellular Electron Transfer and Enrichment of Exoelectrogenic Bacteria in Bioelectrochemical Systems. *Biotechnol Biofuels* **2019**, *12*. [https://doi.org/ARTN 133 10.1186/s13068-019-1477-9](https://doi.org/ARTN%20133%2010.1186/s13068-019-1477-9).
- (27) Kettner, M.; Gohler, B.; Zacharias, H.; Mishra, D.; Kiran, V.; Naaman, R.; Fontanesi, C.; Waldeck, D. H.; Sek, S.; Pawlowski, J.; et al. Spin Filtering in Electron Transport Through Chiral Oligopeptides. *J Phys Chem C* **2015**, *119* (26), 14542–14547. <https://doi.org/10.1021/jp509974z>.
- (28) Kiran, V.; Mathew, S. P.; Cohen, S. R.; Hernández Delgado, I.; Lacour, J.; Naaman, R. Helicenes—A New Class of Organic Spin Filter. *Adv. Mater.* **2016**, *28* (10), 1957–1962. <https://doi.org/10.1002/adma.201504725>.
- (29) Kumar, A.; Capua, E.; Kesharwani, M. K.; Martin, J. M. L.; Sitbon, E.; Waldeck, D. H.; Naaman, R. Chirality-Induced Spin Polarization Places Symmetry Constraints on Biomolecular Interactions. *PNAS* **2017**, *114* (10), 2474–2478. <https://doi.org/10.1073/pnas.1611467114>.

- (30) Mishra, S.; Poonia, V. S.; Fontanesi, C.; Naaman, R.; Fleming, A. M.; Burrows, C. J. Effect of Oxidative Damage on Charge and Spin Transport in DNA. *J Am Chem Soc* **2019**, *141* (1), 123–126. <https://doi.org/10.1021/jacs.8b12014>.
- (31) Kumar, A.; Capua, E.; Vankayala, K.; Fontanesi, C.; Naaman, R. Magnetless Device for Conducting Three-Dimensional Spin-Specific Electrochemistry. *Angew. Chem.* **2017**, *129* (46), 14779–14782. <https://doi.org/10.1002/ange.201708829>.
- (32) Nogues, C.; R. Cohen, S.; S. Daube, S.; Naaman, R. Electrical Properties of Short DNA Oligomers Characterized by Conducting Atomic Force Microscopy. *Physical Chemistry Chemical Physics* **2004**, *6* (18), 4459–4466. <https://doi.org/10.1039/B410862K>.
- (33) Clarke, T. A.; Edwards, M. J.; Gates, A. J.; Hall, A.; White, G. F.; Bradley, J.; Reardon, C. L.; Shi, L.; Beliaev, A. S.; Marshall, M. J.; et al. Structure of a Bacterial Cell Surface Decaheme Electron Conduit. *P Natl Acad Sci USA* **2011**, *108* (23), 9384–9389. <https://doi.org/10.1073/pnas.1017200108>.
- (34) Edwards, M. J.; Baiden, N. A.; Johs, A.; Tomanicek, S. J.; Liang, L. Y.; Shi, L.; Fredrickson, J. K.; Zachara, J. M.; Gates, A. J.; Butt, J. N.; et al. The X-Ray Crystal Structure of *Shewanella Oneidensis* OmcA Reveals New Insight at the Microbe-Mineral Interface. *Febs Lett* **2014**, *588* (10), 1886–1890. <https://doi.org/10.1016/j.febslet.2014.04.013>.
- (35) Kabsch, W.; Sander, C. Dictionary of Protein Secondary Structure - Pattern-Recognition of Hydrogen-Bonded and Geometrical Features. *Biopolymers* **1983**, *22* (12), 2577–2637. [https://doi.org/DOI 10.1002/bip.360221211](https://doi.org/DOI%2010.1002/bip.360221211).
- (36) Firer-Sherwood, M.; Pulcu, G. S.; Elliott, S. J. Electrochemical Interrogations of the Mtr Cytochromes from *Shewanella*: Opening a Potential Window. *J Biol Inorg Chem* **2008**, *13* (6), 849. <https://doi.org/10.1007/s00775-008-0398-z>.
- (37) Hwang, E. T.; Orchard, K. L.; Hojo, D.; Beton, J.; Lockwood, C. W. J.; Adschiri, T.; Butt, J. N.; Reisner, E.; Jeuken, L. J. C. Exploring Step-by-Step Assembly of Nanoparticle:Cytochrome Biohybrid Photoanodes. *ChemElectroChem* **2017**, *4* (8), 1959–1968. <https://doi.org/10.1002/celec.201700030>.

Supporting Information

Spin-Dependent Electron Transport through Bacterial Cell Surface Multiheme Electron Conduits

Suryakant Mishra,^{†#} Sahand Pirbadian,^{‡#} Amit Kumar Mondal,[†] Mohamed Y. El-Naggar,^{*,‡,||§} and Ron Naaman^{*,†}

[†] Department of Chemical and Biological Physics, Weizmann Institute of Science, Rehovot 76100, Israel

[‡] Department of Physics and Astronomy, University of Southern California, Los Angeles, California 90089, United States

^{||} Department of Chemistry, University of Southern California, Los Angeles, California 90089, United States

[§] Department of Biological Sciences, University of Southern California, Los Angeles, California 91030, United States

Experimental details:

Hall Device Fabrication: AlGa_N/Ga_N substrates (from NTT) were used to fabricate the Hall devices. The 3-inch-diameter wafer is composed of a nucleation layer, an 1800-nm-thick intrinsic-GaN (i-GaN) layer, a 20-nm-thick intrinsic-AlGa_N (i-AlGa_N) layer, and a 2-nm-thick capping layer (Figure S1). All the Hall devices were prepared by standard photolithography in a class 1000 clean room. These devices are composed of six electrodes: one source (S) and one drain (D) electrode for constant charge carrier flow, and two pairs of Hall probes to measure the Hall potential. To prepare ohmic contacts, a metallic multilayer, i.e. Ti (20 nm)/Al (100nm)/Ni (40 nm)/Au (40 nm), was annealed at 850°C. A 500 μm × 40 μm region which is the active area of the channel was coated with 2 nm Ti and 5 nm Au for protein adsorption. After adsorption of the protein monolayer (see below), the device chip was glued to a chip holder and device electrodes were connected to the chip holder pads using wire bonding. In addition, a high-quality RTV silicone glue was used to insulate all the connections and pads of the device to avoid charge leakage. To maintain the aqueous environment during the measurements, we prepared a PDMS (polydimethylsiloxane) cell with a 200-μL capacity that was glued on top of the device on the chip holder.

Protein Preparation: OmcA and MtrF with recombinant tetra-cysteine tags were purified as described previously (Wigginton et al, 2007, *Geochimica et Cosmochimica Acta*, and Byun et al, 2014, *ChemElectroChem*), and stored in a 20 mM HEPES-buffered solution containing protease inhibitor, 10% glycerol, 250 mM NaCl, 1% octyl β-D-glucopyranoside (OGP), and 5 mM β-mercaptoethanol at pH 7.6, -80°C. Before preparing the protein solution for the experiment, an additional 2.5 mM β-mercaptoethanol was added, and the solution was incubated for 15 min at 4°C. This solution was then exchanged twice with fresh buffer solution containing 20 mM OGP and 50 mM HEPES using Amicon Ultra-0.5 mL centrifugal filters (10

kDa molecular weight cut-off) at 14,000 rcf and 10°C. The solution was then diluted fivefold with deionized water and placed on the Hall device channel.

Protein Monolayer Formation: Before depositing the protein on the Hall device channel, the device surface was cleaned by boiling acetone and boiling ethanol (10 min each). The surface then underwent UV/OX treatment for 15 min, and was subsequently immersed in ethanol for 30 min. Immediately after, the surface was dried with N₂ stream and the prepared protein solution (described above) was drop cast on the device. The device was then incubated for 16 hours at 4°C in humid environment, and was subsequently rinsed and the PDMS cell was filled with a buffer containing 0.1 M HEPES (and an additional 0.1 M NaCl in the electrochemical experiments).

Denaturation of Protein Monolayer: To thermally denature the protein monolayer, the Hall device was kept at 80°C for one hour, which should be sufficient to denature the protein secondary structure.

Hall Voltage Measurement: The Hall voltage (V_H) in both the polarization and electrochemical experiments was recorded using a Keithley 2182A nanovoltmeter. In order to correct for the error caused by the asymmetry of the Hall device, Hall voltage was measured while constant current was maintained in both directions, i.e., from S to D and D to S. The Hall potential was then calculated by adding the results, $\Delta V_H = V_{HSD} - V_{HDS}$.

Polarization Experiment: A glass coverslip coated with 100 nm of gold was used as the gate electrode, and was placed on top of the PDMS cell that contained a 0.1 M HEPES buffer solution, with the gold-coated side facing away from the solution. A constant potential pulse of different magnitudes was applied to the gold-coated coverslip (with respect to the device channel), providing the electric field that polarized the proteins. During the experiment, a constant current of 10 μ A was maintained between the source (S) and drain (D) electrodes. The varying gate voltages and the constant S-D current were applied using a dual channel Keithley 2636A source measuring unit. All measurements were performed in a dark Faraday cage.

Electrochemical Experiment: The 3-electrode electrochemical setup was composed of the Hall device channel as the working electrode, a Ag/AgCl reference electrode (0.1 M NaCl), and a platinum wire counter electrode. A PalmSens4 electrochemical workstation was used to make the cyclic voltammetry measurements. Similar to the polarization experiment, a constant current of 10 μ A was maintained between the source (S) and drain (D) electrodes. The buffer used during the electrochemical experiments contained 0.1 M HEPES and 0.1 M NaCl. All cyclic voltammetry measurements were performed at a scan rate of 100 mV/s unless stated otherwise.

Magnetic-AFM Experiment: Magnetic field-dependent current vs. voltage (I - V) characteristics of MtrF and OmcA were obtained using a multimode magnetic scanning probe microscopy (SPM) system built with Beetle Ambient AFM and an electromagnet equipped with R9 electronics controller (RHK Technology). Voltage spectroscopy for I - V measurements were performed by applying voltage ramps on a platinum tip (DPE-XSC11, μmasch with spring constant $3\text{-}5.6\text{ Nm}^{-1}$) in contact with the sample at an applied force of 3 nN . At least ~ 80 , I - V curves were scanned in an applied magnetic field of 0.50 T for both UP and DOWN magnetic field orientations. The error was calculated as the standard deviation of all current values measured at each voltage.

Hall Device Calibration using External Magnetic Field: Hall device calibration was done using a superconducting electromagnet, by varying the magnetic field from -500 Oe to $+500\text{ Oe}$ and measuring the corresponding Hall potential across the probes when constant current ($10\text{ }\mu\text{A}$) flowed between S and D.

PMIRRAS Characterization: Polarization modulation-infrared reflection-absorption spectroscopy (PM-IRRAS) was used to characterize the protein monolayers. Nicolet 6700 FTIR equipped with a PEM-90 photoelastic modulator (Hinds Instruments, Hillsboro, OR) at an incidence angle of 80° was used for this measurement.

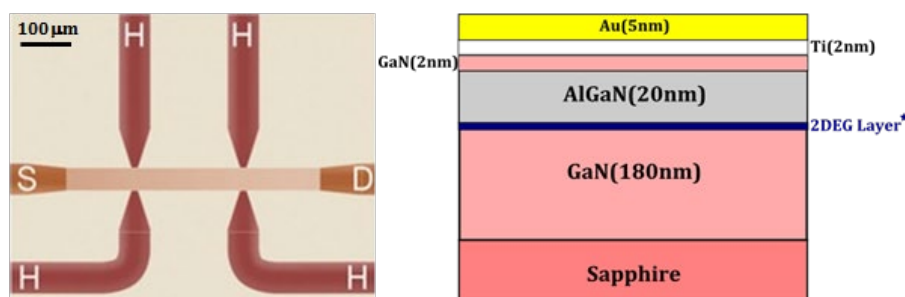


Figure: S1 (a) Optical microscopy image of the HEMT device showing the $500\text{-}\mu\text{m}$ -long channel; the Hall probes are separated from each other by $40\text{ }\mu\text{m}$. **(b)** Composition of the Hall device channel. The top gold layer facilitates the protein adsorption.

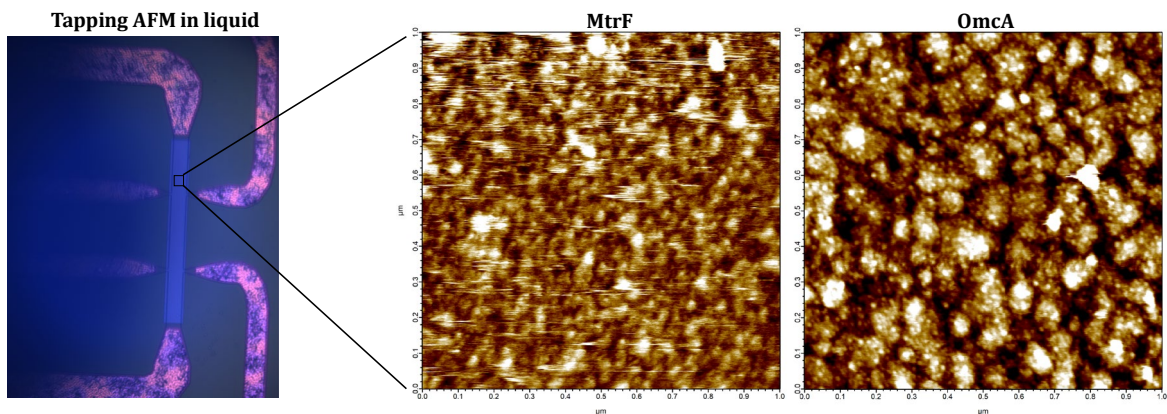


Figure: S2 Optical image of the Hall device (left), along with liquid tapping AFM image of the MtrF monolayer on the Hall device channel (center), and OmcA monolayer on an e-beam deposited gold surface (right).

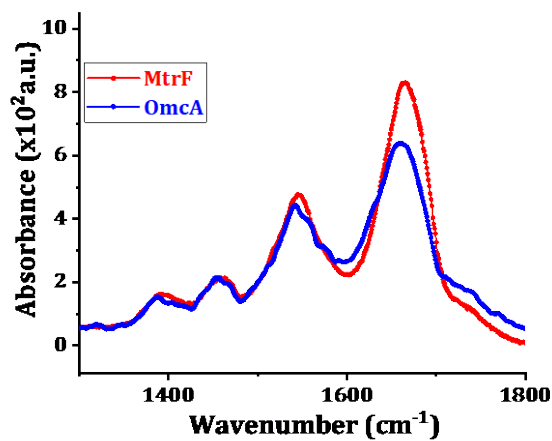


Figure: S3 PMIRRAS spectra of MtrF and OmcA monolayers on a gold surface.

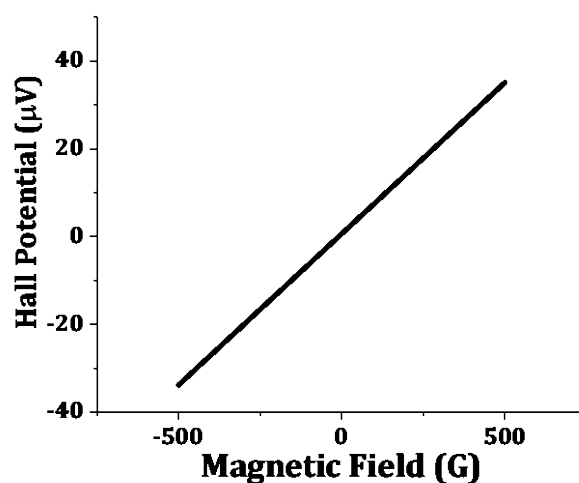


Figure: S4 Hall device calibration using standard magnetic field.

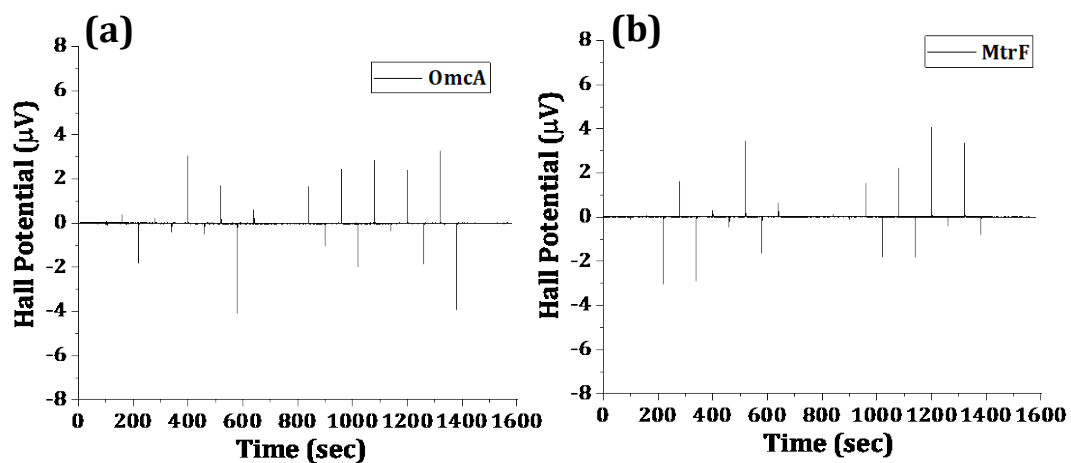


Figure: S5 Polarization data recorded after denaturation for (a) OmcA and (b) MtrF

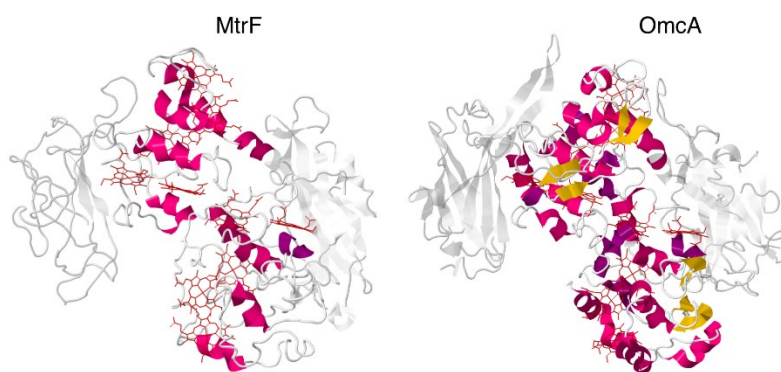


Figure: S6 Crystal structures of MtrF and OmcA, highlighting their heme groups and the helical content in the heme-containing domains II and IV.

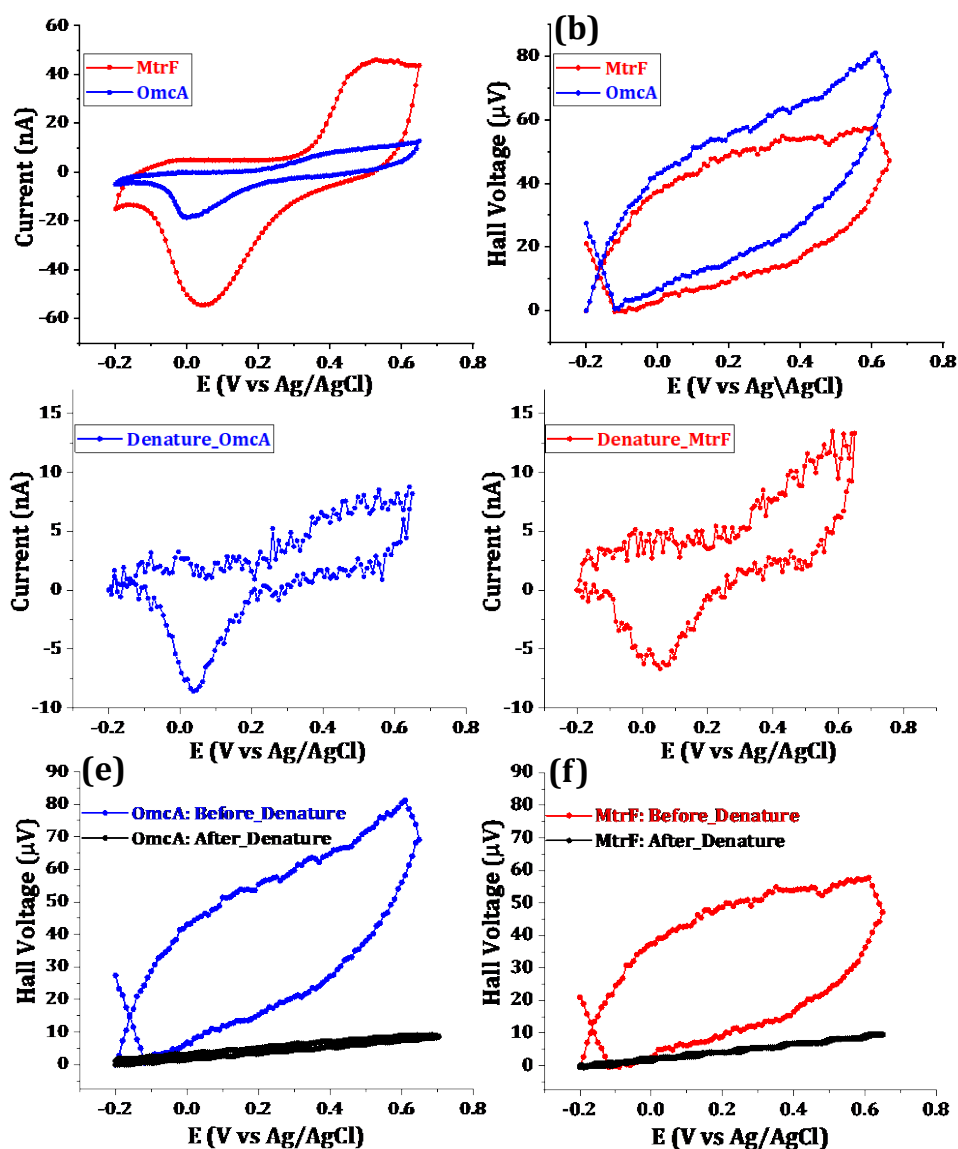


Figure: S7 Electrochemical measurements when the Hall device serves as the working electrode (see Fig. 1d of manuscript). Cyclic voltammetry plot recorded on 100 mV/sec in HEPES buffer+0.1M NaCl. (a) CV plots of MtrF (red) and OmcA (blue). (b) Corresponding Hall potential. Electrochemical data recorded after denaturation (c, d) cyclic voltammetry of denatured OmcA and MtrF recorded at 100mV/s (e, f) corresponding Hall potentials before and after denaturation.

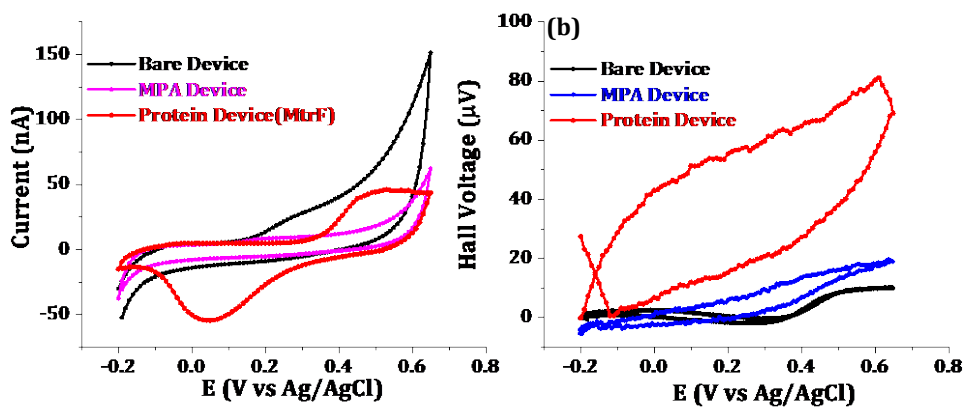


Figure: S8 Device performance check: **(a)** Cyclic voltammetry curves recorded on bare, achiral (3-Mercaptopropionic acid-MPA), and protein (MtrF)-coated device, and **(b)** the corresponding Hall potential.